Plasticized Ionic Liquid Crystal Elastomer Emulsion Based Polymer Electrolyte for Lithium-Ion Batteries

Zakaria Siddiquee , Hyunsang Lee , Weinan Xu , Thein Kyu , Antal Jákli *

Posted Date: 16 February 2025

doi: 10.20944/preprints202502.1144.v1

Keywords: Lithium-battery; Solid-state battery; Polymer electrolyte; Liquid crystal; Ionic liquid crystal elastomer; Plasticizer; Alignment

 doi:10.20944/preprints202502.1144.v1

Article

Plasticized Ionic Liquid Crystal Elastomer Emulsion Based Polymer Electrolyte for Lithium-Ion Batteries

Zakaria Siddiquee [1], Hyunsang Lee [2], Weinan Xu [2], Thein Kyu [2] and Antal Jákli [3,*]

[1] Department of Physics, Kent State University, Kent, OH 44242, USA

[2] School of Polymer Science and Polymer Engineering, University of Akron, Akron, Ohio 44325, USA

[3] Materials Science Graduate Program and Advanced Materials and Liquid Crystal Institute, Kent, OH 44242, USA

* Correspondence: ajakli@kent.edu

Abstract: Development and electrochemical characteristics of ionic liquid crystal elastomers (iLCEs) are described for use as electrolyte components in lithium-ion batteries. The unique combination of elastic and liquid crystal properties in iLCEs grants them robust mechanical attributes and structural ordering. Specifically, the macroscopic alignment of phase-segregated, ordered nanostructures in iLCEs serves as ion pathways, which can be solidified through photopolymerization to create ion-conductive solid-state polymer lithium batteries (SSPLBs) with high ionic conductivity (1.76×10^{-3} S cm^{-1} at 30 °C), and high (0.61) transference number. Additionally, the rubbery state ensures good interfacial contact with electrodes that inhibits lithium dendrite formation. Furthermore, in contrast to liquid electrolytes, the iLCE is shrinking on heating thus preventing any overheating related explosion. The fabricated Li/$LiFePO_4$ (LFP) cells using iLCE-based solid electrolytes show excellent cycling stability with a discharge capacity of ~124 mAh g^{-1} with coulombic efficiency close to 100%. These results are promising for practical application of iLCE-based SSPLBs.

Keywords: Lithium-battery; Solid-state battery; Polymer electrolyte; Liquid crystal; Ionic liquid crystal elastomer; Plasticizer; Alignment

1. Introduction

There is a pressing need to enhance electrolytes in lithium-ion batteries by exploring alternative materials to satisfy the energy, power, and safety demands of electrical energy storage systems [1–21]. Inorganic ceramic electrolytes (ICE) [22–24], solid polymer electrolytes (SPE) [25–30], and recently, polymer electrolyte membranes (PEM) have emerged as potential candidates for high-power, high-energy-density electrochemical-energy storage systems [10,11,18–20,31–38]. Compared to liquid electrolytes, solid polymer electrolytes are known to have lower ionic conductivities (approximately 10^{-8} to 10^{-6} S cm^{-1}) due to their long chains and amorphous structure. To improve the ion conduction, it is a common practice to dissociate the Li salt into a Li cation and a counter organic anion [31,32]. Additionally, dinitrile derivatives (NC−(CH2)n−CN) as plasticizers such as succinonitrile (SCN, n = 2), glutaronitrile (GLN, n = 3), and adiponitrile (ADN, n = 4), that can ionize the salt as well as solubilize ionic species, are used to expedite ion mobility to a level of 10^{-4} – 10^{-3} S cm^{-1} at room temperature [39–48]. The plasticizing strategy further affords to decrease the glass transition temperature (T_g) of the polymer matrix by enhancing segmental chain dynamics, which in turn, promotes higher ion conduction. Currently, polyethylene oxide (PEO) based materials are the leading choice for polymer hosts in PEMs due to PEO's high dielectric constant, excellent ability to solvate Li^+ ions, and favorable chain flexibility. Additionally, PEO is valued for its ease of preparation, cost-effectiveness, reasonable electrochemical stability, and safety features. However, standard linear PEO-based PEMs typically show low ionic conductivities (≤ 10^{-4} S cm^{-1}) at room temperature (RT) by virtue of the high crystallinity of the PEO chains [49–51]. To improve ionic conductivities various

 doi:10.20944/preprints202502.1144.v1

approaches, such as block copolymer electrolytes [52,53], crosslinked polymer electrolytes [54,55], interpenetrating network polymer electrolytes [56], and composite polymer electrolytes [57], have been proposed with promising results. Despite this, most PEO-based PEMs exhibit lithium-ion transference numbers (the fraction of the total electric current carried in an electrolyte by a positive ion) below 0.4. To achieve acceptable battery performance, solid-state polymer lithium batteries (SSPLBs) using these PEMs generally need to operate at around 60 °C, because of their limited ionic conductivities and high electrode/electrolyte interfacial resistances [58].

Consequently, it is essential to develop an optimized PEM with highly selective Li^+ transport characteristics both in bulk and at interfaces to enable SSPLBs to function effectively at room temperature (RT). The concept of using fluid ionic liquid crystals (iLCs) with ion channels as ion conductive films and liquid iLCs based batteries has been proposed before and has been shown that imidazolium salts in iLCs can form liquid crystals for long enough alkyl chains [59–65].

In this study, we explore the potential of ionic liquid crystal elastomers (iLCEs) [66], as a novel promising PEM constituent, which, to the best of our knowledge, is the first study to demonstrate the potential practical application of solid ionic liquid crystal elastomers (iLCE)-based SSPLBs. The appeal of iLCEs lies in their ability to maintain orientational order over a wide temperature range and their capacity to contract at increasing temperatures [67], thereby reducing pressure on electrode surfaces or interfaces. Their organized ion pathways can be solidified through photopolymerization to create nanostructured ion-conductive electrolyte networks [68–70]. Additionally, integrating succinonitrile (SCN) into the well-defined iLCE structures can significantly enhance Li^+ transport efficiency [71,72]. Based on this concept, we developed a freestanding and flexible solid electrolyte through in situ photopolymerization of iLCE/SCN/lithium bis(trifluoromethyl sulfonyl)imide (LiTFSI) for use in ambient temperature SSPLBs (**Figure S4**). The resulting iLCE-based PEM exhibits exceptional electrochemical properties, including high ionic conductivity, excellent compatibility with electrodes and effective suppression of lithium dendrite growth.

2. Results

Experimental Section/Methods are described in the Supporting Information (SI).

2.1. Material Composition

Monofunctional acrylate monomer 4-(6-Acryloxy-hex-1-yl-oxy) phenyl-4-(hexyloxy) benzoate (M1) and bifunctional monomer 1,4-Bis-[4-(6-acryloyloxyhexyloxy) benzoyloxy]-2-methylbenzene (M2) were purchased from Synthon chemicals. Ionic liquid 1-Hexyl-3-methylimidazolium bis(trifluormethyl sulfonyl)imide (HMIM-TFSI), photoinitiator 2,2-Dimethoxy-2-phenylacetophenone (Irgacure® 651), ionic salt lithium bis(trifluoromethyl sulfonyl)imide (LITFSI), plasticizer succinonitrile (SCN) were acquired from Sigma-Aldrich, Milwaukee, US. Lithium metal disks (about 600 μm thick) and lithium iron phosphate (LFP) were purchased from MSE supplies (**Error! Reference source not found.**).

 doi:10.20944/preprints202502.1144.v1

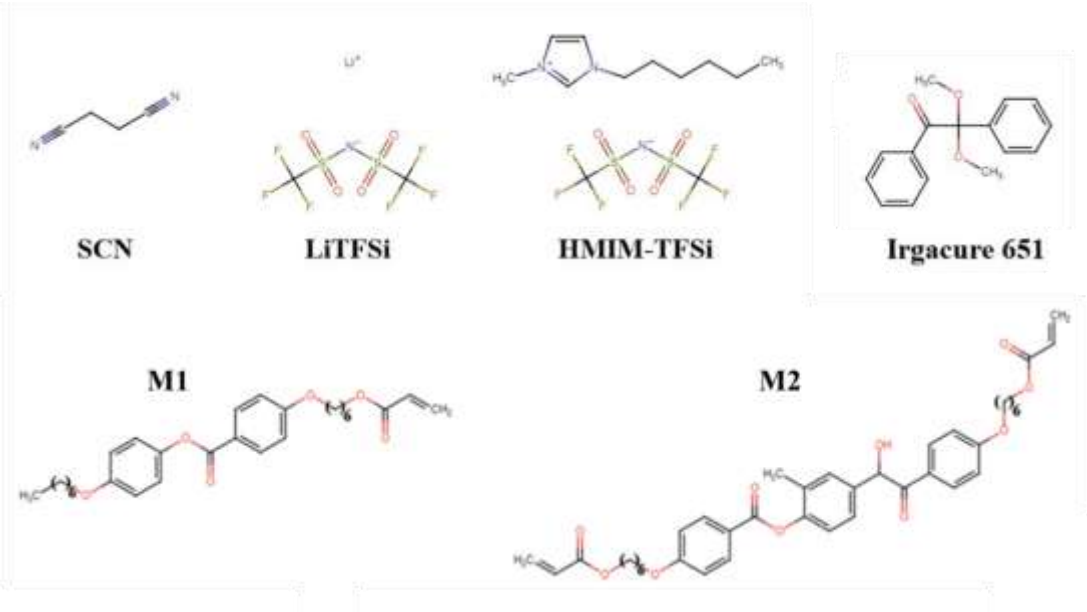

Figure 1. The molecular structures of the components of the studied PEM: M1 and M2 are mesogenic units. HMIM-TFSI is the ionic liquid, Irgacure 651 is the photoinitiator, SCN is the plasticizer, LiTFSI is the ionic salt.

2.1.1. Synthesis of Ionic Liquid Crystal Elastomer

M1, M2, and the photoinitiator were mixed in 87:12:1 weight ratio to form the LCE precursors (see **Figure S6**(a)), because it gave the optimum LCE properties [66,68–72]. Subsequently, an ionic liquid (HMIM-TFSI) was added to the LCE precursor solution and mechanically stirred for 24 *h* using a magnetic stirrer in an Ar-filled glovebox after heating to 80 ºC to achieve complete mixing. The mixture was then stored in a glass amber vial to prevent photopolymerization and kept in the glovebox at room temperature for future use. **Figure S6** shows a synthesis route of UV crosslinking reaction between M1 and M2 functional groups using a 1 wt% Irgacure 651 photoinitiator to obtain LCE co-networks. The same reaction was undertaken in the presence of LiTFSI salt and SCN plasticizer that afforded a transparent, homogeneous film before and after UV curing, suggestive of a miscible character among the PEM constituents.

2.1.2. Fabrication of iLCE Electrolyte Membrane

The binary eutectic mixture of LiTFSI and SCN at weight ratios of 25:50 was melt-mixed at 60 ºC under Ar-gas environment. Subsequently, the homogeneously dissolved LiTFSI and SCN binary mixture was further mixed with the pre-mixed iLCE precursors at various wt% for an additional 24 *h*. The SPE membrane based on iLCE was prepared through UV photopolymerization of iLCE, SCN, and LiTFSI. The homogeneous mixture was poured into a polytetrafluoroethylene mold with a thickness of 300 μm and a diameter of 15 mm approximately, where the solution was kept at various preset temperatures for 0.5 *h*. Subsequently, the electrolyte membrane was exposed to 365 nm UV light at 280 mW cm^{-2} intensity for 30 *s* at the pre-set temperatures to activate the photoinitiator to polymerize the mono- and bi-functional LCE monomers. These functional groups reacted in the presence of SCN plasticizer and LiTFSI salt in various ratios. Upon curing, a binary iLCE co-network-based electrolyte membrane (PEM) was formed with a film thickness of approximately 300 μm. Finally, the flexible electrolyte films were dried at RT under vacuum for 24 *h*. Fourier Transform Infrared Spectroscopy (FTIR) was performed on the electrolyte film and on the individual components to check the formation of fully cross-linked LCE co-networks, as shown in **Figure S1**.

 doi:10.20944/preprints202502.1144.v1

Error! Reference source not found. shows SEM images of the electrolyte film. As SEM is carried out in vacuum, the low molecular weight components (ionic liquids) are evaporated, and their former places appear dark. This way we get information about the distribution of the ionic channels that is crucial for the operation of the battery. The images in **Error! Reference source not found.**(a, c) show that the ionic liquid and the polymers form bi-continuous structure, thus allowing ionic pathway from one end to the other. The diameter of the ion channels varies from 40 μm (see **Error! Reference source not found.**(a, b)) down to 100 nm range as seen in **Error! Reference source not found.**(d). **Error! Reference source not found.**(b) illustrates phase separated polymer (LCE and SCN) domains. The minority component (LCE) phase separates into spherical shape droplets from the continuous majority component (SCN) – more evidence on this is shown by POM (**Error! Reference source not found.**(a-d)), as will be discussed in later sections. Importantly, **Error! Reference source not found.**(d), where we see a part of the minority droplet, shows that ion channels interpenetrate even in the discontinuous minority domain.

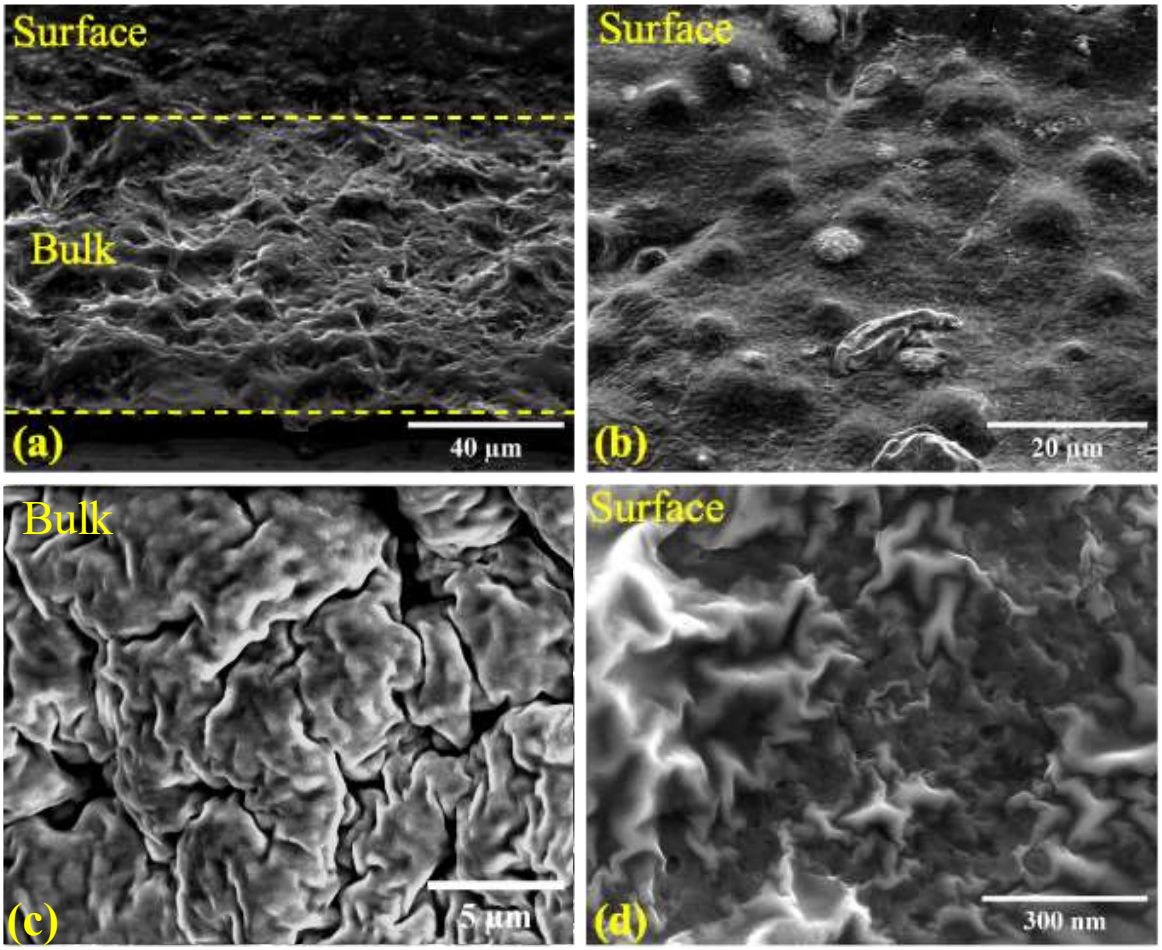

Figure 2. SEM images of the iLCE SPE. (a) Electrolyte cross-section tilted at 45º, (b) Surface image, (c) Bulk image at electrolyte cross-section, (d) Zoomed in texture on the surface of liquid crystal droplet.

2.2. Electrochemical Performance

An impedance test for various PEM compositions was performed from 20 ºC to 100 ºC using a homemade rectangular cell having an area of 1mm × 1mm and a 0.1 mm gap. The ionic conductivity $\sigma(T)$ for each PEM composition was found to decrease with increasing temperature in reasonably good approximation following Arrhenius behavior, $\sigma(T) \propto \exp\left(-\frac{E_a}{k_B T}\right)$, where $k_B = 1.38 \times 10^{-23}$ J K^{-1}, T is the temperature in Kelvin scale, and E_a is the activation energy. **Figure 1** shows the electric conductivity as a function of $10^3/T$ for various LCE (**Figure 1**(a)), SCN (**Figure 1**(b)), ionic liquid (IL)

 doi:10.20944/preprints202502.1144.v1

and Li^+ ratios (**Figure 1**(c)), and at various crosslink temperatures (**Figure 1**(d)). The straight lines are the best fits corresponding to the Arrhenius behavior.

In comparison of 30, 40 and 50 % of LCE contents (**Figure 1**(a)), one finds that the highest ionic conductivity values (9.0×10^{-4} S cm^{-1} at 20 ºC, and 5.39×10^{-3} S cm^{-1} at 90 – 100 ºC) were found for 30 % LCE. The activation energies obtained from the slopes of the best fits are 0.12, 0.27 and 0.44 eV for the 30, 40 and 50 % of LCE contents, respectively. This means the material is becoming increasingly solid at increasing LCE concentration.

The effect of a plasticizer on lithium-ion conduction was examined by comparing 10, 20, 30, 40, 50 wt% SCN, keeping the liquid crystal elastomer composition to be the same (**Figure 1**(b)). It is found that the ionic conductivity is increasing with increasing SCN concentration below 30 wt%. This is because an increasing plasticizer amount enhances the polymer chain dynamics, promoting ion conductions from an anode to a cathode and vice versa [31–33,42]. At higher SCN concentrations the conductivity saturates providing about the same conductivity for the 40 and 50 wt% SCN. In accordance with the enhanced polymer chain dynamics, the activation energies decrease from 0.22 eV to 0.16 eV between 10% to 30 % plasticizer concentrations. However, at excessive plasticizer amount of SCN (> 40 wt%) the activation energies are higher (0.22 and 0.19 eV at 40 and 50 wt%, respectively) indicating phase separation between the iLCE and SCN and the small-molecule weight SCN tends to ooze out to the PEM surface. This phase separation interrupts the ion channels that leads to saturation (an even slight decrease) of the conductivity and an increase of the activation energy.

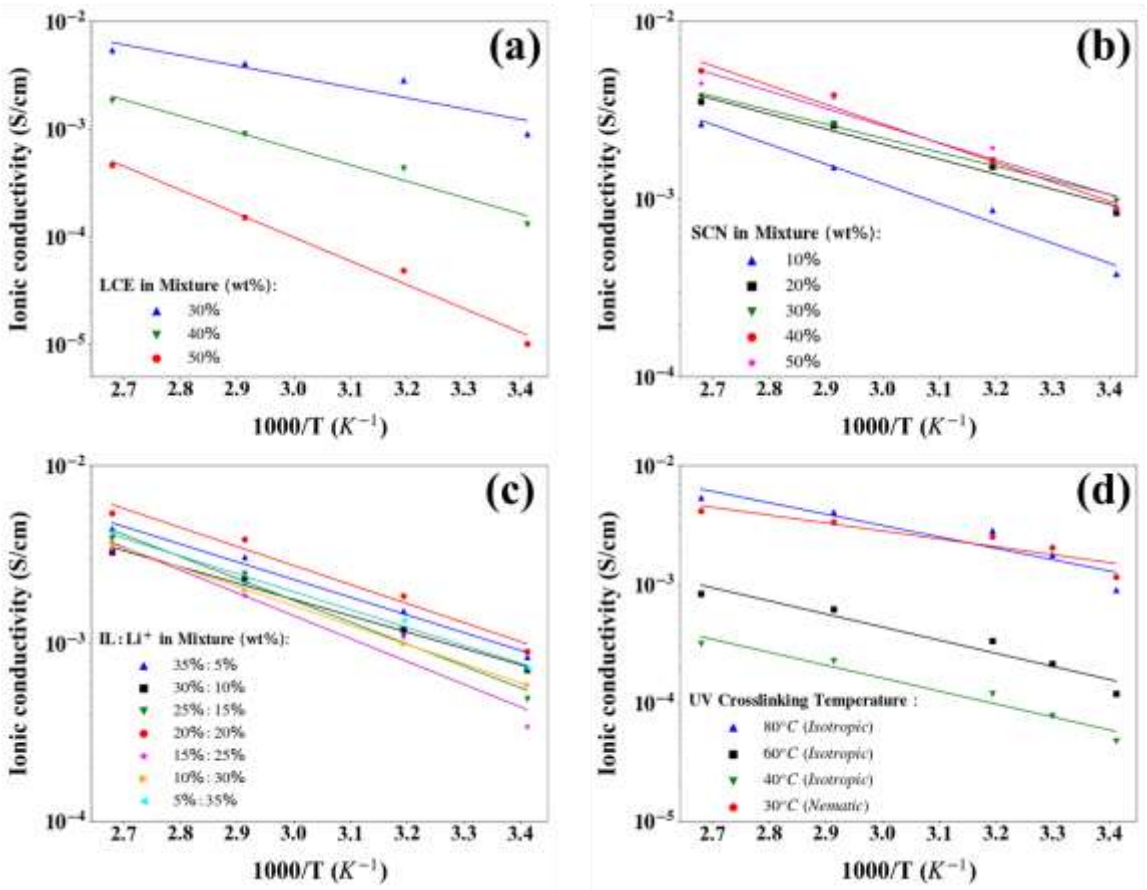

Figure 1. Arrhenius plots of ionic conductivity (logarithmic conductivity versus 1000/T). (a) For different ratios of LCE in electrolyte mixture; (b) For different ratios of SCN in electrolyte mixture; (c) For different ratios of HMIM-TFSI and LiTFSI in electrolyte mixture; and (d) For different crosslinking temperature of PEM.

The effect of the ionic liquid (IL) to Li salt ratio on the ionic conductivity was investigated by comparing the 5:35, 10:30, 15:25, 20:20, 25:15, 30:10 and 35:5 IL:Salt ratios so that the total weight percentage added to 40 wt% of the total mixture, keeping the same amounts of SCN and LCE (**Figure**

 doi:10.20944/preprints202502.1144.v1

1(c)). At room temperature the ionic conductivity of the 20:20 IL-LiTFSI PEM was the largest, 1.76 × 10^{-3} S cm^{-1}. The activation energies are found to be 0.20, 0.18, 0.24, 0.21, 0.26, 0.22 and 0.20 eV for the 5:35, 10:30, 15:25, 20:20, 25:15, 30:10 and 35:5 IL:Salt ratios, respectively.

The effect of polymerization temperature on the ionic conduction was examined by polymerizing in the nematic phase of the liquid crystal at 30 ºC and in the isotropic phase at 40, 60, 80 °C, during UV irradiation (**Figure 1**(d)). Comparing samples polymerized in the isotropic phase, we find that at room temperature the ionic conductivity increases with increasing polymerization temperatures, most likely due to decreased cross-link density toward higher polymerization temperatures. Interestingly, the conductivity of the sample polymerized in the nematic phase is even higher than that of the PEM polymerized at 80 °C. This suggests that the elastomer network in the nematic phase forms a directional network which in turn acts as ion conduction pathways for improved ion conduction. The slopes of the best fits gave 0.19, 0.22, 0.22, 0.13 eV for the samples polymerized in 30, 40, 60, 80 °C, respectively.

Based on these findings, subsequent experiments were focused on the LCE/HMIM-TFSI/LiTFSI/SCN: 30/17.5/17.5/35 PEM, as it showed the highest (1.76 × 10^{-3} S cm^{-1}) ionic conductivity at ambient temperature. Such conductivity value is comparable to those of lower end organic liquid electrolyte batteries [34–36]. We conservatively chose this composition containing lower LCE content due to its mechanical integrity during assembling. Moreover, at room temperature this chosen 30/17.5/17.5/35 PEM exhibits an ion transference number (the ratio of the electric current derived from the cation to the total electric current) of t_+ ~ 0.61, which is considerably higher than those (0.22 - 0.35) of organic electrolyte systems, suggesting the domination of ion transport by lithium cations over the TFSI anion [40] (**Figure 2**).

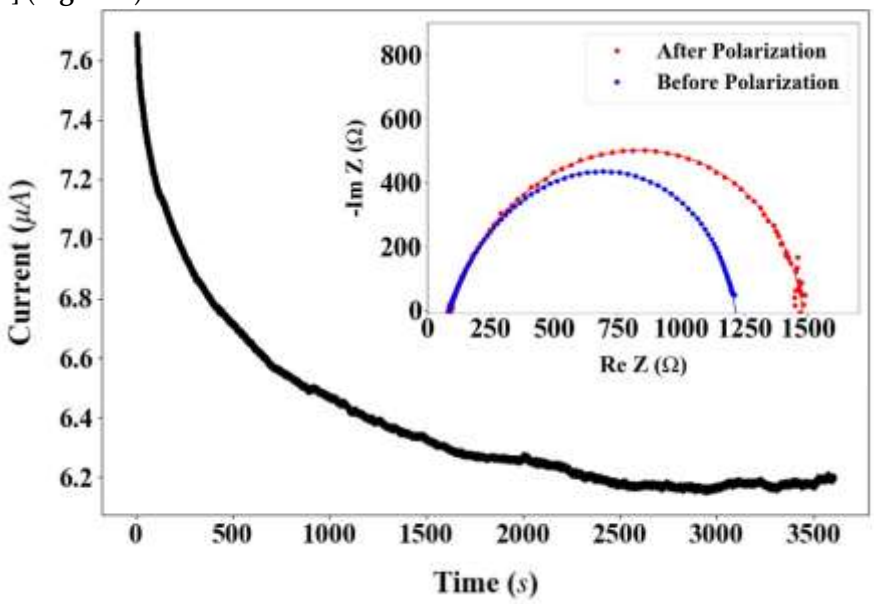

Figure 2. Chronoamperometry of a symmetric (Li–PEM–Li) cell at ambient temperature in response to a U_{DC}=0.01 V bias for the LCE/HMIM-TFSI/LiTFSI/SCN:30/17.5/17.5/35 PEM. The inset shows the Nyquist plot of the PEM impedance before DC polarization and after steady-state current conditions.

To determine the transference number of lithium ions through the PEMs, Li/PEM/Li symmetric coin cells were assembled and measured by using Autolab PGSTAT302N galvanostat. A constant DC bias of 10 mV was applied to determine the initial (I_0) and steady-state (I_S) currents, and the response of current was monitored for 3600 *s* until a steady-state current was reached. The before (R_0) and after (R_S) resistances of PEMs were determined by means of an impedance analyzer in the frequency range from 1 Hz to 100 kHz. The transference number (t_+) of the PEMs was calculated in accordance with the following equation: $t_+ = \frac{I_S(\Delta V - I_0 R_0)}{I_0(\Delta V - I_S R_S)}$, where ΔV is the DC polarization voltage applied through the PEMs.

 doi:10.20944/preprints202502.1144.v1

2.3. Structure of iLCE electrolytes

Polarized Optical Microscopy (POM) studies before and after cross-linking, and inspection of mechanical properties of the LCE/HMIM-TFSI/LiTFSI/SCN: 30/17.5/17.5/35 PEM are shown in **Error! Reference source not found.**. POM studies showed that the mixture before crosslinking is in the isotropic phase above 34.2 °C; it has a nematic phase between 34 °C and 24 °C and it is crystalline below 24 °C. **Error! Reference source not found.**(a, b) show POM images of a 20 μm film between two bare glass plates (no rubbing) before polymerization under cross polarizers in the isotropic (60 °C) and nematic (31 °C) phase, respectively. The isotropic structure is evidenced by the uniformly dark image. In the nematic phase, the iLC prepolymer and the SCN plasticizer phase separate and form a structure like polymer dispersed nematic liquid crystals (PDLCs) [73]. The droplets exhibit four dark brushes (so-called Maltese crosses) along the cross polarizers indicating that the LC director orients either tangentially or radially inside the droplets [74]. Because of the radial symmetry, the optical texture remains unchanged when the sample is rotated between the crossed polarizers. After UV induced crosslinking, the PDLC-type structure remains unchanged although the size of the iLCE micro droplets depends on the UV intensity, polymerization time and temperature. At 280 mW cm^{-2} UV intensity applied at 60 °C for 30 *s* cross linking time the packing of iLCE droplets is quite dense with droplets sizes approximately 3 - 10 μm as shown in **Error! Reference source not found.**(c). After polymerization, the iLCE electrolyte shows a nematic phase between 34 °C and 56 °C. At higher temperatures, the droplets become isotropic, but the overall structure does not change, and on cooling the nematic droplets appear again in their original locations. Heating above 110 ºC will start to melt the electrolyte membrane to liquid.

Error! Reference source not found.(d) shows the surface structure without polarizers after low intensity slow (10 mW cm^{-2} for 10 min) polymerization. One can see that slow polymerization causes uneven distribution of droplet sizes and occasionally forms large domains of iLCEs in SCN matrix. Thus, we opted for fast polymerization at high intensities. **Error! Reference source not found.**(e, f) show 300 μm thick free-standing films of the 30/17.5/17.5/35 PEM at room temperature. In **Error! Reference source not found.**(e) one can see that the 300 μm thick film is self-standing and solid, while **Error! Reference source not found.**(f) demonstrates that the iLCE PEM is flexible. The toughness of a 2 mm × 1 cm × 1cm (m ~ 0.262 g) thick film was tested by hanging weights of up to 60 g masses when it started tearing up, as shown in **Figure S2**.

 doi:10.20944/preprints202502.1144.v1

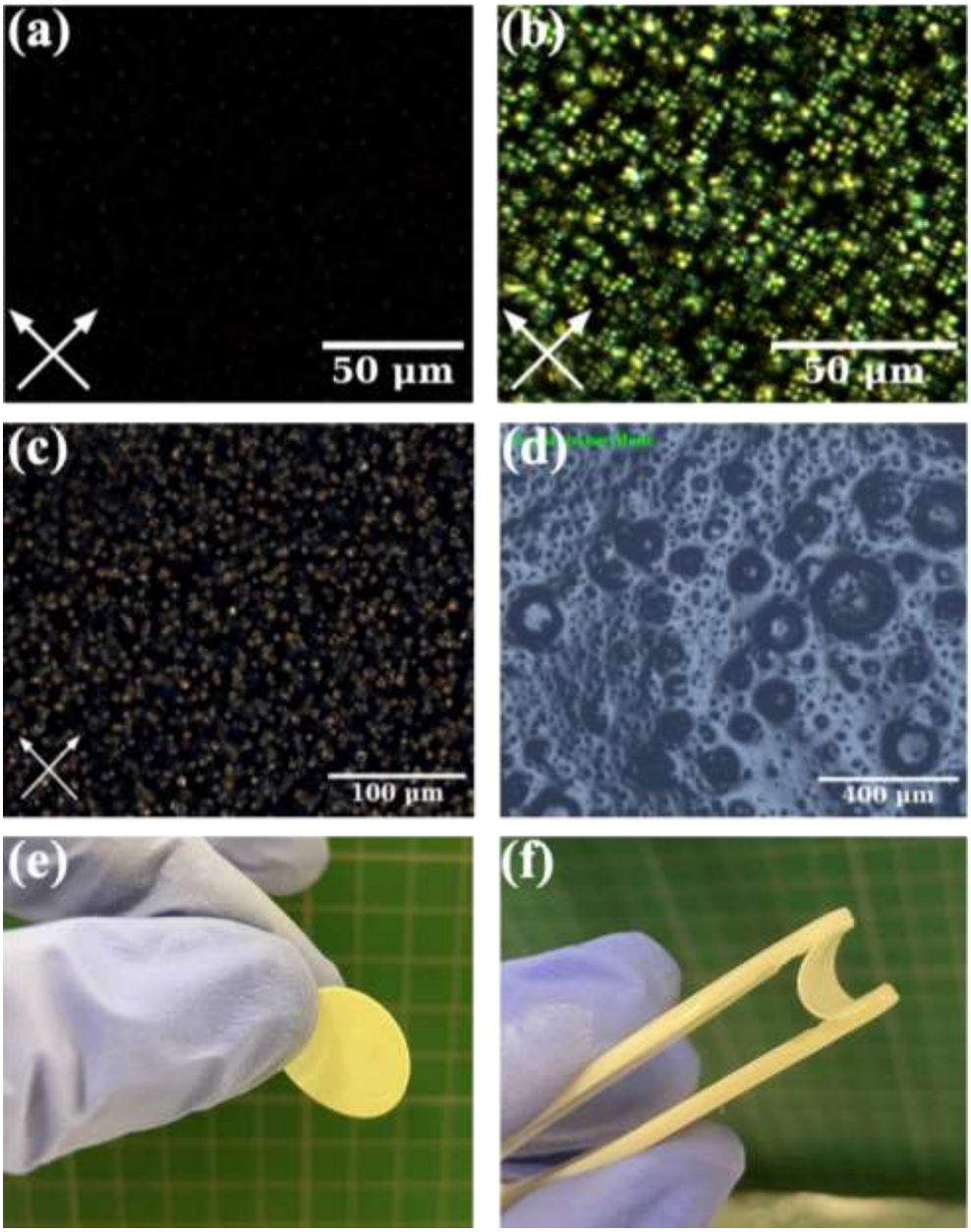

Figure 5. Polarized Optical Microscopy (POM) studies before (a, b) and after (c) cross-linking, Microscopy image of the surface after (d) cross-linking and inspection of mechanical properties (e, f) of the 30/17.5/17.5/35 PEM after cooling at 0.1 ºC min^{-1} rate. (a) POM image in the isotropic phase at 60 ºC, (b) Nematic droplets at 31 °C. (c) Nematic elastomer droplets after crosslinking by 280 mW cm^{-2} UV intensity at 80 ºC applied for 30 *s*; (d) Surface images of nematic elastomer droplets after crosslinking by 10 mW cm^{-2} for **10 *min***. between parallel polarizers (e) Self-standing 300 µm thick film; (f) Demonstration of the flexibility of the iLCE PEM film.

2.4. Cell Performance

To understand the Li-ion storage mechanism in the PEM during prelithiation, cyclic voltammetry (CV) and galvanometric charge/discharge cyclic tests were carried out in Li metal/PEM/$LiFePO_4$ (LFP) configuration using CR2032 coin cells at various potential ranges 2.5 - 4.0 V. In the linear sweep voltammetry (LSV) scans, PEMs appear stable against the stainless-steel (SS) electrode up to 3.7 V (see **Error! Reference source not found.**(a)), as indicated by the arrows at the onsets of the CV curves (see **Error! Reference source not found.**(b)). The PEM's stability up to 3.75 V in LSV data (**Error! Reference source not found.**(a)) likely indicates a stability limitation, which is typical for organic and polymer electrolytes [75,76].

 doi:10.20944/preprints202502.1144.v1

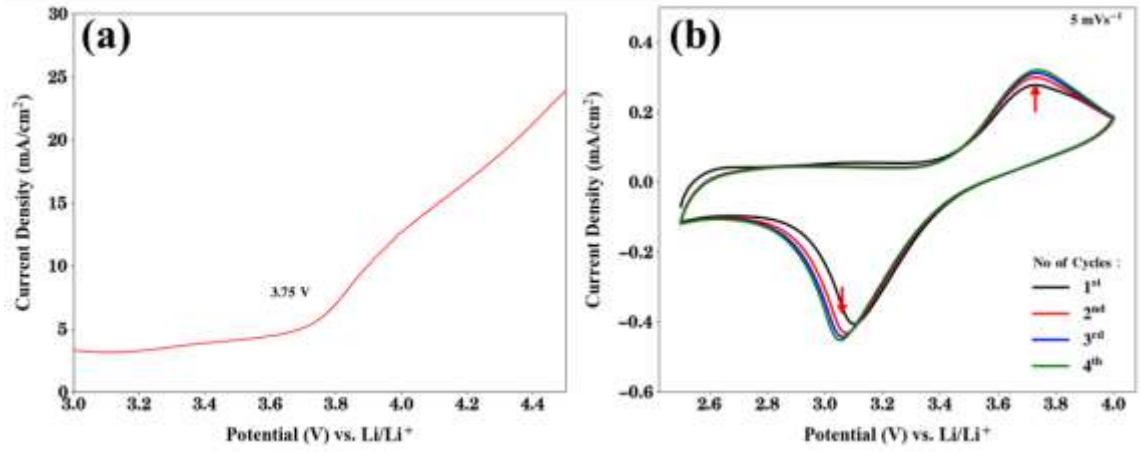

Figure 6. Summary of voltammetry results with potential scan rate of 5 mV s^{-1}. (a) Linear sweep voltammogram of PEM at 24 °C, (b) Cyclic voltammetry test of the Li/SPE/LFP configuration in cathode range (2.5 - 4.0 V) at 24 °C.

To identify the origin of oxidation and reduction peaks, a full battery cell was assembled in the Li-metal anode, /SPE/LFP cathode configuration based on 30/17.5/17.5/35 LCE/HMIM-TFSI/LiTFSI/SCN PEM composition. When the CV test was carried out in 2.5 V to 4.0 V range using the LFP cathode, the oxidation and reduction peaks of the Li-metal anode and those of PEM can be observed in the corresponding potential ranges, which continue to increase from the 2nd to the 4th cycles. As can be expected, the oxidation and reduction peaks of the LFP cathode are observable in the vicinity of 3.6 V ~ 4.0 V and 3.0 V, respectively, which fluctuates slightly with increasing number of cycles (**Error! Reference source not found.**(b)). The continued increase in the peak strength may be attributed to the continued lithiation occurring in situ during repeated cycles, hereafter termed "in situ lithiation". More importantly, these CV results are indeed reproducible, although the resulting oxidation and reduction peaks could increase or decrease depending on the competition between the in situ lithiation versus the capacity fading.

To further confirm the electrochemical stability of a PEM-based rechargeable battery, the galvanometric charge/discharge cycling test was performed at 0.1C rate from 3.0 V to 3.7 V (**Error! Reference source not found.**(a, b)). Note, XY C-Rate means X Current × Y Hours the battery can provide X current. The initial specific capacity was ~124 mAh g^{-1} which dropped to ~100 mAh g^{-1} with the capacity retention of about 80% and the Coulombic efficiency of ~99 %. To avoid any potential overcharging issues in the LFP cathode, the test was operated up to 3.7 V instead of 4.0 V.

 doi:10.20944/preprints202502.1144.v1

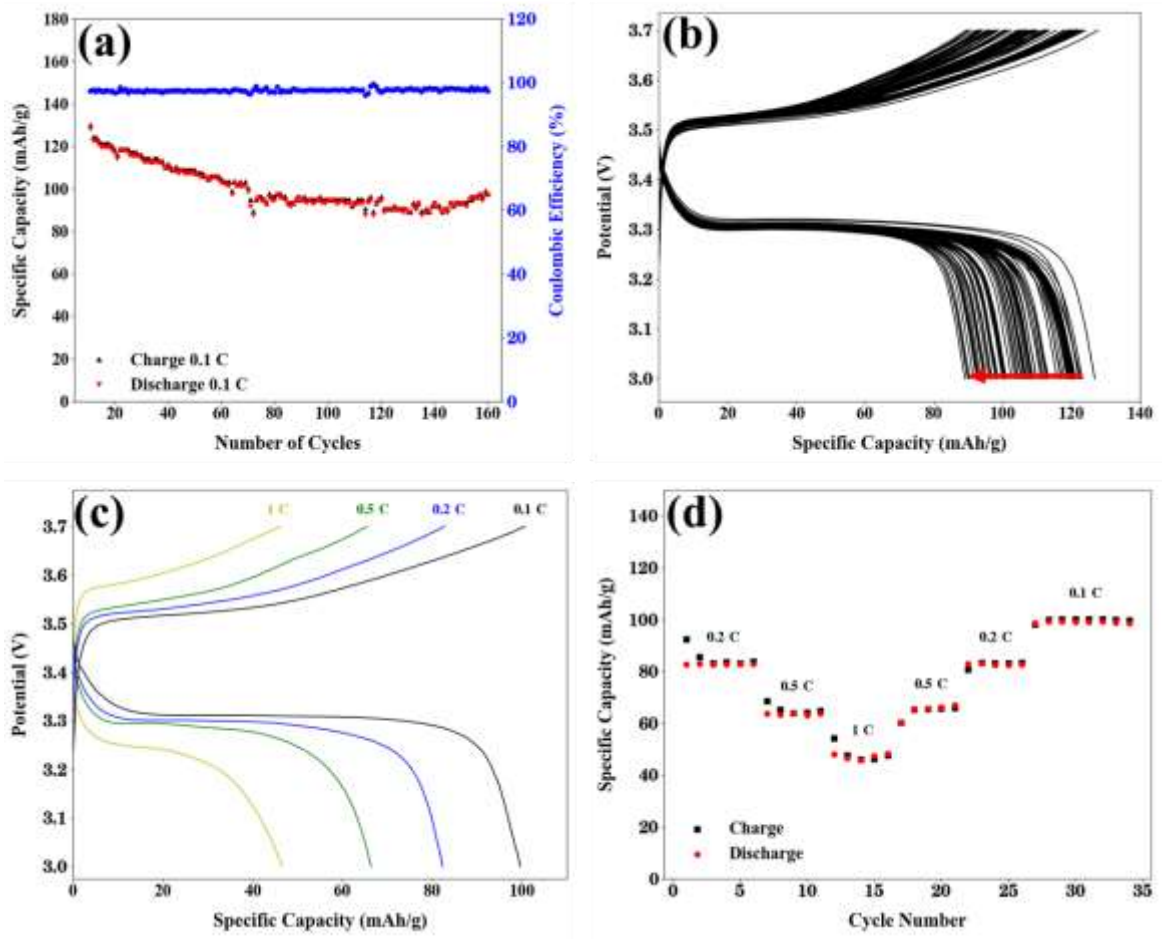

Figure 7. Charge and discharge cycling characteristics of the iLCE based PEM in coin cell battery. (a) Specific capacity and coulombic efficiency over 160 charge and discharge cycles; (b) Charge and discharge profiles for Li/SPE/LFP cathode cells with a cathode range of 3.0-3.7V at a C-rate of 0.1 at 25 °C; (c) Charge/discharge curves of Li/SPE/LFP cell at different C-rates after 100 cycles; (d) The cycle performance of the Li/SPE/LFP battery during galvanostatic cycling at 0.1, 0.2, 0.5 and 1 C-rate.

Error! Reference source not found.(c, d) show the charge/discharge voltage profiles and capability of the PEM at different C-rates. The cell clearly delivers outstanding average discharge capacities of 98.2, 83.4, 65.7, and 48.8 mAh g^{-1} at C-rates of 0.1, 0.2, 0.5, and 1 at room temperature, respectively. It can be observed that the cell exhibits excellent reversibility and the charge–discharge capacities are almost the same at a given C-rate. Unfortunately, the cell exhibits poor performance at higher C-rates. According to the manufacturer, the specific capacity of the LFP sheet used as the cathode is 130 mAh g^{-1}, which is only slightly larger than the initial 124 mAh g^{-1} we obtained. A challenge arises from the interaction between the nitrile groups in the SCN plasticizer and the lithium metal anode. Li^0 can catalyze nitrile polymerization, leading to side reactions at the anode, potentially affecting cathodic stability [77]. Additionally, our composite electrolyte functions as a dual-ion conductor, with a non-unity transference number. This implies that lithium ions at the interface may be consumed or generated faster than they can migrate, creating a salt concentration gradient. Such a gradient can deplete the salt at the electrode, increasing ionic resistance, or cause salt precipitation due to enrichment. Despite this, cyclic voltammetry results and post charge-discharge analysis show minimal evidence of a salt gradient forming during operation. At 0.1 C-rate from cycles 80 to 160, the iLCE/LiTFSI/SCN cell maintained a discharge capacity of around 98.8 mAh g^{-1} with nearly perfect coulombic efficiency (~99%). The stable interfacial properties and excellent capacity retention are largely attributed to the flexibility of the ILC-based electrolyte film, which ensures long-term cycling stability at room temperature.

 doi:10.20944/preprints202502.1144.v1

3. Conclusions

We designed and then successfully prepared the first liquid crystal elastomer-based free-standing and flexible ambient temperature SSPLB through in situ photopolymerization of LCE/HMIM-TFSI/LiTFSI/SCN. The iLCE-based PEM exhibits high ionic conductivity (1.76×10^{-3} S cm^{-1} at 30 ºC) and an electrochemical window of 3.7 V. The iLCE based PEM delivered a high ionic transference number (0.61) because iLCE could construct ion-conductive channels for more efficient transport of Li^+. These outstanding comprehensive electrochemical properties enabled the iLCE-based PEM LFP/Li cells to maintain a capacity of 98.8 mAh g^{-1} after 160 cycles under 0.1 C-rate at RT with over 80% specific capacity retention and ~ 99 % coulombic efficiency. The excellent rate capability and low temperature performance of the cell has also been confirmed. We believe all the above excellent properties, along with the easy fabrication process, enable the iLCE-based PEM to have excellent potential for RT solid-state LIBs with high capacity and safety. This study presents the first and most promising results for a room temperature SSPLB utilizing an ionic liquid crystal elastomer-based PEM. Future work will focus on the alignment effects of the iLCE based solid electrolytes.

As we were preparing our work for submission, we became aware of a study by Wang et al utilizing LCE in batteries [78]. Their electrolyte exhibited a room-temperature conductivity comparable to ours at 2 mS cm^{-1}. However, while they employed RM257 as the sole LC mesogenic unit, our approach incorporated both mono- and bi-functional mesogenic units, M1 and M2, respectively. Additionally, unlike our study, their formulation did not include plasticizers. Structurally, our LC formed nematic droplets, whereas theirs resulted in a polydomain LC film. In cyclic voltammetry, their oxidation and reduction peaks were observed at 4.03 V and 3.20 V, respectively, whereas ours appeared around 3.75 V and 3.04 V. The transference number across their various samples ranged from 0.57 to 0.72, while our system exhibited a value of 0.61. Regarding battery performance, a key distinction between Wang et al and our work lies in the number of oxygen sites in the polymer chains. In polymer electrolytes, ion hopping is a primary mode of ion transport, relying on oxygen sites [79,80]. Notably, lithium binding to oxygen in the polymer electrolyte membrane (PEM) may enhance the overall capacity beyond the theoretical maximum of the cathode's active material [81]. The study by Wang et al [78] incorporated carbon-based additives such as PVDF as a binder and acetylene black, whereas our cathode was purely $LiFePO_4$ (LFP)-based, explaining the specific capacity disparity between our systems aside from different ionic liquid cation interaction with Li-salt.

4. Patents

A Utility - Provisional Application under 35 USC 111(b) entitled “Solid State Battery Including Ionic Liquid Crystal Elastomers” has been filed by Zakaria Siddiquee, Hyunsang Lee, Weinan Xu, Thein Kyu and Antal Jákli on 10/10/2024 by Application #: 63/705,869, Attorney Docket #: KSU.605.PRV.

Supplementary Materials: The following supporting information can be downloaded at the website of this paper posted on Preprints.org. Supporting Information is available from the www.mdpi.com or from the author.

Author Contributions: Conceptualization, A.J. Methodology, T.K and W.X.; validation, Z.S. and H.L.; formal analysis, Z.S.; investigation, Z.S.; resources, T.K., W.X. and A.J.; data curation, Z.S. and H.L.; writing—original draft preparation, Z.S.; writing—review and editing, A.J., T.K. and W.X.; supervision, A.J. All authors have read and agreed to the published version of the manuscript.

Funding: This research received no external funding.

Data Availability Statement: The data that support the findings of this study are available from the corresponding author upon reasonable request.

Acknowledgments: Z.S and A.J. acknowledge useful discussions with Dr. Paul Rajib.

 doi:10.20944/preprints202502.1144.v1

Conflicts of Interest: The authors declare no conflicts of interest.

References

1. Holtstiege, F.; Bärmann, P.; Nölle, R.; Winter, M.; Placke, T. Pre-Lithiation Strategies for Rechargeable Energy Storage Technologies: Concepts, Promises and Challenges. *Batteries* 2018, *4*, 4.
2. Herr, R. Organic Electrolytes for Lithium Cells. *Electrochim Acta* **1990**, *35*, doi:10.1016/0013-4686(90)90059-9.
3. Aurbach, D.; Ein-Eli, Y.; Markovsky, B.; Zaban, A.; Luski, S.; Carmeli, Y.; Yamin, H. The Study of Electrolyte Solutions Based on Ethylene and Diethyl Carbonates for Rechargeable Li Batteries: II . Graphite Electrodes. *J Electrochem Soc* **1995**, *142*, 2882–2889, doi:10.1149/1.2048659.
4. Walker, C.W.; Cox, J.D.; Salomon, M. Conductivity and Electrochemical Stability of Electrolytes Containing Organic Solvent Mixtures with Lithium Tris(Trifluoromethanesulfonyl)Methide. *J Electrochem Soc* **1996**, *143*, L80–L82, doi:10.1149/1.1836607.
5. Armand, M. The History of Polymer Electrolytes. *Solid State Ion* **1994**, *69*, 309–319, doi:10.1016/0167-2738(94)90419-7.
6. Alloin, F.; Sanchez, J.Y.; Armand, M. New Solvating Cross-Linked Polyether for Lithium Batteries. *J Power Sources* **1995**, *54*, 34–39, doi:10.1016/0378-7753(94)02036-3.
7. Goodenough, J.B.; Kim, Y. Challenges for Rechargeable Li Batteries. *Chemistry of Materials* 2010, *22*, 587–603.
8. Etacheri, V.; Marom, R.; Elazari, R.; Salitra, G.; Aurbach, D. Challenges in the Development of Advanced Li-Ion Batteries: A Review. *Energy Environ Sci* 2011, *4*, 3243–3262.
9. Chu, S.; Majumdar, A. Opportunities and Challenges for a Sustainable Energy Future. *Nature* 2012, *488*, 294–303.
10. Goodenough, J.B.; Park, K.S. The Li-Ion Rechargeable Battery: A Perspective. *J Am Chem Soc* 2013, *135*, 1167–1176.
11. Tatsumisago, M.; Nagao, M.; Hayashi, A. Recent Development of Sulfide Solid Electrolytes and Interfacial Modification for All-Solid-State Rechargeable Lithium Batteries. *Journal of Asian Ceramic Societies* 2013, *1*, 17–25.
12. Armand, M.; Tarascon, J.M. Building Better Batteries. *Nature* 2008, *451*, 652–657.
13. Tarascon, J.M.; Armand, M. Issues and Challenges Facing Rechargeable Lithium Batteries. *Nature* 2001, *414*, 359–367.
14. Nair, J.R.; Imholt, L.; Brunklaus, G.; Winter, M. Lithium Metal Polymer Electrolyte Batteries: Opportunities and Challenges. *Electrochemical Society Interface* **2019**, *28*, 55–61, doi:10.1149/2.F05192if.
15. Deng, K.; Qin, J.; Wang, S.; Ren, S.; Han, D.; Xiao, M.; Meng, Y. Effective Suppression of Lithium Dendrite Growth Using a Flexible Single-Ion Conducting Polymer Electrolyte. *Small* **2018**, *14*, 231424, doi:10.1002/smll.201801420.
16. Zhang, H.; Li, C.; Piszcz, M.; Coya, E.; Rojo, T.; Rodriguez-Martinez, L.M.; Armand, M.; Zhou, Z. Single Lithium-Ion Conducting Solid Polymer Electrolytes: Advances and Perspectives. *Chem Soc Rev* 2017, *46*, 797–815.
17. Shono, K.; Kobayashi, T.; Tabuchi, M.; Ohno, Y.; Miyashiro, H.; Kobayashi, Y. Proposal of Simple and Novel Method of Capacity Fading Analysis Using Pseudo-Reference Electrode in Lithium Ion Cells: Application to Solvent-Free Lithium Ion Polymer Batteries. *J Power Sources* **2014**, *247*, 1026–1032, doi:10.1016/j.jpowsour.2013.06.071.
18. Nakayama, M.; Wada, S.; Kuroki, S.; Nogami, M. Factors Affecting Cyclic Durability of All-Solid-State Lithium Polymer Batteries Using Poly(Ethylene Oxide)-Based Solid Polymer Electrolytes. *Energy Environ Sci* **2010**, *3*, 1995–2002, doi:10.1039/c0ee00266f.
19. Kaneko, F.; Wada, S.; Nakayama, M.; Wakihara, M.; Koki, J.; Kuroki, S. Capacity Fading Mechanism in All Solid-State Lithium Polymer Secondary Batteries Using PEG-Borate/Alumlnate Ester as Plasticizer for Polymer Electrolytes. *Adv Funct Mater* **2009**, *19*, 918–925, doi:10.1002/adfm.200800789.
20. Fergus, J.W. Ceramic and Polymeric Solid Electrolytes for Lithium-Ion Batteries. *J Power Sources* 2010, *195*, 4554–5469.

21. Goodenough, J.B. Batteries and a Sustainable Modern Society. *Electrochemical Society Interface* **2016**, *25*, 67, doi:10.1149/2.F05163if.
22. Yu, X.; Manthiram, A. A Review of Composite Polymer-Ceramic Electrolytes for Lithium Batteries. *Energy Storage Mater* 2021, *34*, 282–300.
23. Li, S.; Zhang, S.Q.; Shen, L.; Liu, Q.; Ma, J. Bin; Lv, W.; He, Y.B.; Yang, Q.H. Progress and Perspective of Ceramic/Polymer Composite Solid Electrolytes for Lithium Batteries. *Advanced Science* 2020, *7*, 1903088.
24. Chung, S.H.; Wang, Y.; Persi, L.; Croce, F.; Greenbaum, S.G.; Scrosati, B.; Plichta, E. Enhancement of Ion Transport in Polymer Electrolytes by Addition of Nanoscale Inorganic Oxides. In Proceedings of the Journal of Power Sources; 2001; Vol. 97–98, pp. 644–648.
25. Takeda, Y.; Yamamoto, O.; Imanishi, N. Lithium Dendrite Formation on a Lithium Metal Anode from Liquid, Polymer and Solid Electrolytes. *Electrochemistry* **2016**, *84*, 210–218, doi:10.5796/electrochemistry.84.210.
26. Wang, D.; Zhang, W.; Zheng, W.; Cui, X.; Rojo, T.; Zhang, Q. Towards High-Safe Lithium Metal Anodes: Suppressing Lithium Dendrites via Tuning Surface Energy. *Advanced Science* **2017**, *4*, 1600168, doi:10.1002/advs.201600168.
27. Mandal, M.; Bardhan, P.; Mandal, M.; Maji, T.K. Development of Wood Polymer Composites with Thermosetting Resin from Soybean Oil Cross-Linked with Rosin Derivative. *European Journal of Wood and Wood Products* **2020**, *78*, 1265–1278, doi:10.1007/s00107-020-01564-3.
28. Goydaragh, M.G.; Taghizadeh-Mehrjardi, R.; Jafarzadeh, A.A.; Triantafilis, J.; Lado, M. Using Environmental Variables and Fourier Transform Infrared Spectroscopy to Predict Soil Organic Carbon. *Catena (Amst)* **2021**, *202*, 105280, doi:10.1016/j.catena.2021.105280.
29. Ehgartner, C.R.; Werner, V.; Selz, S.; Hüsing, N.; Feinle, A. Carboxylic Acid-Modified Polysilsesquioxane Aerogels for the Selective and Reversible Complexation of Heavy Metals and Organic Molecules. *Microporous and Mesoporous Materials* **2021**, *312*, 110759, doi:10.1016/j.micromeso.2020.110759.
30. Evans, J.; Vincent, C.A.; Bruce, P.G. Electrochemical Measurement of Transference Numbers in Polymer Electrolytes. *Polymer (Guildf)* **1987**, *28*, 2324–2328, doi:10.1016/0032-3861(87)90394-6.
31. Bruce, P.G.; Evans, J.; Vincent, C.A. Conductivity and Transference Number Measurements on Polymer Electrolytes. *Solid State Ion* **1988**, *28–30*, 918–922, doi:10.1016/0167-2738(88)90304-9.
32. Strickberger, S.A.; Ravi, S.; Daoud, E.; Niebauer, M.; Man, K.C.; Morady, F. Relation between Impedance and Temperature during Radiofrequency Ablation of Accessory Pathways. *Am Heart J* **1995**, *130*, 1026–1030, doi:10.1016/0002-8703(95)90204-X.
33. Feng, C.; Kyu, T. Role of Dinitrile Plasticizer Chain Lengths in Electrochemical Performance of Highly Conductive Polymer Electrolyte Membrane for Lithium Ion Battery. *Electrochim Acta* **2020**, *330*, 135320, doi:10.1016/j.electacta.2019.135320.
34. Pal, U.; Chen, F.; Gyabang, D.; Pathirana, T.; Roy, B.; Kerr, R.; MacFarlane, D.R.; Armand, M.; Howlett, P.C.; Forsyth, M. Enhanced Ion Transport in an Ether Aided Super Concentrated Ionic Liquid Electrolyte for Long-Life Practical Lithium Metal Battery Applications. *J Mater Chem A Mater* **2020**, *8*, 18826–18839, doi:10.1039/d0ta06344d.
35. Chang, Z.; Qiao, Y.; Deng, H.; Yang, H.; He, P.; Zhou, H. A Liquid Electrolyte with De-Solvated Lithium Ions for Lithium-Metal Battery. *Joule* **2020**, *4*, 1776–1789, doi:10.1016/j.joule.2020.06.011.
36. Sun, H.; Zhu, G.; Zhu, Y.; Lin, M.C.; Chen, H.; Li, Y.Y.; Hung, W.H.; Zhou, B.; Wang, X.; Bai, Y.; et al. High-Safety and High-Energy-Density Lithium Metal Batteries in a Novel Ionic-Liquid Electrolyte. *Advanced Materials* **2020**, *32*, 2001741, doi:10.1002/adma.202001741.
37. Kobayashi, K.; Pagot, G.; Vezzù, K.; Bertasi, F.; Di Noto, V.; Tominaga, Y. Effect of Plasticizer on the Ion-Conductive and Dielectric Behavior of Poly(Ethylene Carbonate)-Based Li Electrolytes. *Polym J* **2021**, *53*, 149–155, doi:10.1038/s41428-020-00397-4.
38. Wang, B.; Wu, Y.; Zhuo, S.; Zhu, S.; Chen, Y.; Jiang, C.; Wang, C. Synergistic Effect of Organic Plasticizer and Lepidolite Filler on Polymer Electrolytes for All-Solid High-Voltage Li-Metal Batteries. *J Mater Chem A Mater* **2020**, *8*, 5968–5974, doi:10.1039/c9ta14239h.

39. Rosero-Navarro, N.C.; Kajiura, R.; Miura, A.; Tadanaga, K. Organic–inorganic Hybrid Materials for Interface Design in All-Solid-State Batteries with a Garnet-Type Solid Electrolyte. *ACS Appl Energy Mater* **2020**, *3*, 11260–11268, doi:10.1021/acsaem.0c02164.
40. Onozuka, R.; Piedrahita, C.; Yanagida, Y.; Adachi, K.; Tsukahara, Y.; Kyu, T. Ion Conductive Polymer Electrolyte Membranes Based on Star-Branched Poly(Ethylene-Glycol Tri-Acrylate) and Polysulfide Macromonomers. *Solid State Ion* **2020**, *346*, 115182, doi:10.1016/j.ssi.2019.115182.
41. He, R.; Peng, F.; Dunn, W.E.; Kyu, T. Chemical and Electrochemical Stability Enhancement of Lithium Bis(Oxalato)Borate (LiBOB)-Modified Solid Polymer Electrolyte Membrane in Lithium Ion Half-Cells. *Electrochim Acta* **2017**, *246*, 123–134, doi:10.1016/j.electacta.2017.06.043.
42. Piedrahita, C.; Kusuma, V.; Nulwala, H.B.; Kyu, T. Highly Conductive, Flexible Polymer Electrolyte Membrane Based on Poly(Ethylene Glycol) Diacrylate-Co-Thiosiloxane Network. *Solid State Ion* **2018**, *322*, 61–68, doi:10.1016/j.ssi.2018.05.006.
43. Cao, J.; He, R.; Kyu, T. Fire Retardant, Superionic Solid State Polymer Electrolyte Membranes for Lithium Ion Batteries. *Curr Opin Chem Eng* 2017, *15*, 68–75.
44. Fu, G.; Soucek, M.D.; Kyu, T. Fully Flexible Lithium Ion Battery Based on a Flame Retardant, Solid-State Polymer Electrolyte Membrane. *Solid State Ion* **2018**, *320*, 310–315, doi:10.1016/j.ssi.2018.03.021.
45. Fu, G.; Dempsey, J.; Izaki, K.; Adachi, K.; Tsukahara, Y.; Kyu, T. Highly Conductive Solid Polymer Electrolyte Membranes Based on Polyethylene Glycol-Bis-Carbamate Dimethacrylate Networks. *J Power Sources* **2017**, *359*, 441–449, doi:10.1016/j.jpowsour.2017.05.097.
46. Fu, G.; Kyu, T. Effect of Side-Chain Branching on Enhancement of Ionic Conductivity and Capacity Retention of a Solid Copolymer Electrolyte Membrane. *Langmuir* **2017**, *33*, 13973–13981, doi:10.1021/acs.langmuir.7b03449.
47. He, R.; Echeverri, M.; Ward, D.; Zhu, Y.; Kyu, T. Highly Conductive Solvent-Free Polymer Electrolyte Membrane for Lithium-Ion Batteries: Effect of Prepolymer Molecular Weight. *J Memb Sci* **2016**, *498*, 208–217, doi:10.1016/j.memsci.2015.10.008.
48. He, R.; Kyu, T. Effect of Plasticization on Ionic Conductivity Enhancement in Relation to Glass Transition Temperature of Crosslinked Polymer Electrolyte Membranes. *Macromolecules* **2016**, *49*, 5637–5648, doi:10.1021/acs.macromol.6b00918.
49. Ibrahim, S.; Johan, M.R. Conductivity, Thermal and Neural Network Model Nanocomposite Solid Polymer Electrolyte System (PEO-LiPF 6-EC-CNT). *Int J Electrochem Sci* **2011**, *6*, 5565–5587.
50. Klongkan, S.; Pumchusak, J. Effects of Nano Alumina and Plasticizers on Morphology, Ionic Conductivity, Thermal and Mechanical Properties of PEO-LiCF3SO3 Solid Polymer Electrolyte. *Electrochim Acta* **2015**, *161*, 171–176, doi:10.1016/j.electacta.2015.02.074.
51. Christie, A.M.; Lilley, S.J.; Staunton, E.; Andreev, Y.G.; Bruce, P.G. Increasing the Conductivity of Crystalline Polymer Electrolytes. *Nature* **2005**, *433*, 18305–18308, doi:10.1038/nature03186.
52. Phan, T.N.T.; Issa, S.; Gigmes, D. Poly(Ethylene Oxide)-Based Block Copolymer Electrolytes for Lithium Metal Batteries. *Polym Int* 2019, *68*, 7–13.
53. Young, W.S.; Epps, T.H. Ionic Conductivities of Block Copolymer Electrolytes with Various Conducting Pathways: Sample Preparation and Processing Considerations. *Macromolecules* **2012**, *45*, 4689–4697, doi:10.1021/ma300362f.
54. Ben youcef, H.; Garcia-Calvo, O.; Lago, N.; Devaraj, S.; Armand, M. Cross-Linked Solid Polymer Electrolyte for All-Solid-State Rechargeable Lithium Batteries. *Electrochim Acta* **2016**, *220*, 587–594, doi:10.1016/j.electacta.2016.10.122.
55. Stalin, S.; Choudhury, S.; Zhang, K.; Archer, L.A. Multifunctional Cross-Linked Polymeric Membranes for Safe, High-Performance Lithium Batteries. *Chemistry of Materials* **2018**, *30*, 2058–2066, doi:10.1021/acs.chemmater.7b05353.
56. Schulze, M.W.; McIntosh, L.D.; Hillmyer, M.A.; Lodge, T.P. High-Modulus, High-Conductivity Nanostructured Polymer Electrolyte Membranes via Polymerization-Induced Phase Separation. *Nano Lett* **2014**, *14*, 122–126, doi:10.1021/nl4034818.

 doi:10.20944/preprints202502.1144.v1

57. Yang, L.; Wang, Z.; Feng, Y.; Tan, R.; Zuo, Y.; Gao, R.; Zhao, Y.; Han, L.; Wang, Z.; Pan, F. Flexible Composite Solid Electrolyte Facilitating Highly Stable "Soft Contacting" Li–Electrolyte Interface for Solid State Lithium-Ion Batteries. *Adv Energy Mater* **2017**, *7*, 1701437, doi:10.1002/aenm.201701437.
58. Bhattacharyya, A.J.; Fleig, J.; Guo, Y.G.; Maier, J. Local Conductivity Effects in Polymer Electrolytes. *Advanced Materials* **2005**, *17*, 2630–2634, doi:10.1002/adma.200500926.
59. Yoshio, M.; Mukai, T.; Ohno, H.; Kato, T. One-Dimensional Ion Transport in Self-Organized Columnar Ionic Liquids. *J Am Chem Soc* **2004**, *126*, 994–995, doi:10.1021/ja0382516.
60. Yamanaka, N.; Kawano, R.; Kubo, W.; Kitamura, T.; Wada, Y.; Watanabe, M.; Yanagida, S. Ionic Liquid Crystal as a Hole Transport Layer of Dye-Sensitized Solar Cells. *Chemical Communications* **2005**, 740–742, doi:10.1039/b417610c.
61. Lee, S.; Becht, G.A.; Lee, B.; Burns, C.T.; Firestone, M.A. Electropolymerization of a Bifunctional Ionic Liquid Monomer Yields an Electroactive Liquid-Crystalline Polymer. *Adv Funct Mater* **2010**, *20*, 2063–2070, doi:10.1002/adfm.201000024.
62. Wang, S.; Liu, X.; Wang, A.; Wang, Z.; Chen, J.; Zeng, Q.; Wang, X.; Zhang, L. An Ionic Liquid Crystal-Based Solid Polymer Electrolyte with Desirable Ion-Conducting Channels for Superior Performance Ambient-Temperature Lithium Batteries. *Polym Chem* **2018**, *9*, 4674–4682, doi:10.1039/c8py00951a.
63. Mukai, T.; Yoshio, M.; Kato, T.; Yoshizawa, M.; Ohno, H. Anisotropic Ion Conduction in a Unique Smectic Phase of Self-Assembled Amphiphilic Ionic Liquids. *Chemical Communications* **2005**, 1333, doi:10.1039/b414631j.
64. Uchida, Y.; Matsumoto, T.; Akita, T.; Nishiyama, N. Ion Conductive Properties in Ionic Liquid Crystalline Phases Confined in a Porous Membrane. *J Mater Chem C Mater* **2015**, *3*, 6144–6147, doi:10.1039/c5tc00314h.
65. Kuo, D.; Soberats, B.; Kumar, K.R.S.; Yoshio, M.; Ichikawa, T.; Ohno, H.; Zeng, X.; Ungar, G.; Kato, T. Switching of Ionic Conductivities in Columnar Liquid-Crystalline Anilinium Salts: Effects of Alkyl Chains, Ammonium Cations and Counter Anions on Thermal Properties and Switching Temperatures. *Mol Syst Des Eng* **2019**, *4*, 342–347, doi:10.1039/c8me00099a.
66. Feng, C.; Hemantha Rajapaksha, C.P.; Jákli, A. Ionic Elastomers for Electric Actuators and Sensors. *Engineering* 2021, *7*, 581.
67. Luo, S.C.; Sun, S.; Deorukhkar, A.R.; Lu, J.T.; Bhattacharyya, A.; Lin, I.J.B. Ionic Liquids and Ionic Liquid Crystals of Vinyl Functionalized Imidazolium Salts. *J Mater Chem* **2011**, *21*, 1866–1873, doi:10.1039/c0jm02875d.
68. Hemantha Rajapaksha, C.P.; Paudel, P.R.; Kodikara, P.M.S.G.; Dahal, D.; Dassanayake, T.M.; Kaphle, V.; Lüssem, B.; Jákli, A. Ionic Liquid Crystal Elastomers-Based Flexible Organic Electrochemical Transistors: Effect of Director Alignment of the Solid Electrolyte. *Appl Phys Rev* **2022**, *9*, 011415, doi:10.1063/5.0077027.
69. Alyami, A.; Rajapaksha, C.P.H.; Paudel, P.R.; Kaphle, V.; Kodikara, S.G.; Lüssem, B.; Jákli, A. Bending Sensor Using Ionic Liquid Crystal Elastomers as Solid Electrolyte of Organic Electrochemical Transistors. *Liq Cryst* **2023**, 297–304, doi:10.1080/02678292.2023.2297269.
70. Rajapaksha, C.P.H.; Gunathilaka, M.D.T.; Narute, S.; Albehaijan, H.; Piedrahita, C.; Paudel, P.; Feng, C.; Lüssem, B.; Kyu, T.; Jákli, A. Flexo-Ionic Effect of Ionic Liquid Crystal Elastomers. *Molecules* **2021**, *26*, 4234, doi:10.3390/molecules26144234.
71. Feng, C.; Rajapaksha, C.P.H.; Cedillo, J.M.; Piedrahita, C.; Cao, J.; Kaphle, V.; Lüssem, B.; Kyu, T.; Jákli, A. Electroresponsive Ionic Liquid Crystal Elastomers. *Macromol Rapid Commun* **2019**, *40*, 1900299, doi:10.1002/marc.201900299.
72. Alyami, A.; Rajapaksha, C.P.H.; Feng, C.; Paudel, P.R.; Paul, A.; Adaka, A.; Dharmarathna, R.; Lüssem, B.; Jákli, A. Ionic Liquid Crystal Elastomers for Actuators, Sensors, and Organic Transistors. *Liq Cryst* **2023**, *50*, 1151–1161, doi:10.1080/02678292.2023.2188615.
73. Drzaic, P.S. *Liquid Crystal Dispersions*; 1995;
74. Scharf, T. *Polarized Light in Liquid Crystals and Polymers*; 2006;
75. Méry, A.; Rousselot, S.; Lepage, D.; Dollé, M. A Critical Review for an Accurate Electrochemical Stability Window Measurement of Solid Polymer and Composite Electrolytes. *Materials* 2021, *14*.

 doi:10.20944/preprints202502.1144.v1

76. Seidl, L.; Grissa, R.; Zhang, L.; Trabesinger, S.; Battaglia, C. Unraveling the Voltage-Dependent Oxidation Mechanisms of Poly(Ethylene Oxide)-Based Solid Electrolytes for Solid-State Batteries. *Adv Mater Interfaces* **2022**, *9*, doi:10.1002/admi.202100704.
77. Alarco, P.J.; Abu-Lebdeh, Y.; Abouimrane, A.; Armand, M. The Plastic-Crystalline Phase of Succinonitrile as a Universal Matrix for Solid-State Ionic Conductors. *Nat Mater* **2004**, *3*, doi:10.1038/nmat1158.
78. Wang, X.; He, Z.; Yan, R.; Niu, H.; He, W.; Miao, Z. Liquid Crystal Elastomer-Based Solid Electrolyte with Intelligently Regulated Rigidity–Flexibility toward High-Energy Lithium Batteries. *Chemical Engineering Journal* **2025**, *503*, 158552, doi:10.1016/j.cej.2024.158552.
79. Fu, J.; Li, Z.; Zhou, X.; Guo, X. Ion Transport in Composite Polymer Electrolytes. *Mater Adv* 2022.
80. Gerdroodbar, A.E.; Alihemmati, H.; Safavi-Mirmahaleh, S.A.; Golshan, M.; Damircheli, R.; Eliseeva, S.N.; Salami-Kalajahi, M. A Review on Ion Transport Pathways and Coordination Chemistry between Ions and Electrolytes in Energy Storage Devices. *J Energy Storage* 2023, *74*.
81. Lee, H.; Choi, J.W.; Kyu, T. A Comparative Study on Electrochemical Performance of Single versus Dual Networks in Lithium Metal/Polysulfide-Polyoxide Co-Network/Lithium Titanium Oxide Cathode. *Batteries* **2024**, *10*, doi:10.3390/batteries10050163.